

# Visualization of steps and surface reconstructions in Helium Ion Microscopy with atomic precision

Gregor Hlawacek<sup>a,1,2,\*</sup>, Maciej Jankowski<sup>a,3,4</sup>, Herbert Wormeester<sup>a,5</sup>, Raoul van Gastel<sup>a,5</sup>, Harold J. W. Zandvliet<sup>a,5</sup>, Bene Poelsema<sup>a,5</sup>

<sup>a</sup>*Physics of Interfaces and Nanomaterials, University of Twente, PO Box 217, 7500 AE, Enschede, The Netherlands*

---

## Abstract

Helium Ion Microscopy is known for its surface sensitivity and high lateral resolution. Here, we present results of a Helium Ion Microscopy based investigation of a surface confined alloy of Ag on Pt(111). Based on a change of the work function of 25 meV across the atomically flat terraces we can distinguish Pt rich from Pt poor areas and visualize the single atomic layer high steps between the terraces. Furthermore, dechanneling contrast has been utilized to measure the periodicity of the hcp/fcc pattern formed in the 2 ML thick Ag alloy layer. A periodicity of 6.65 nm along the  $\langle\bar{1}\bar{1}2\rangle$  surface direction has been measured. In terms of crystallography a hcp domain is obtained through a lateral displacement of a part of the outermost layer by  $1/\sqrt{3}$  of a nearest neighbour spacing along  $\langle\bar{1}\bar{1}2\rangle$ . The findings are perfectly in line with results obtained with Low Energy Electron Microscopy and Phase Contrast Atomic Force Microscopy.

*Keywords:* Helium Ion Microscopy, Channeling, Surface alloy, Step contrast, Low Energy Electron Microscopy

---

\*Corresponding author

*Email address:* g.hlawacek@hzdr.de (Gregor Hlawacek)

<sup>1</sup>Present address: Ion beam Physics and Materials Research, Helmholtz—Zentrum Dresden – Rossendorf, Bautzner Landstraße 400, 01328, Dresden, Germany

<sup>2</sup>Acquired and analyzed all HIM based data. AFM analysis. Wrote the manuscript.

<sup>3</sup>Present address: ID03 Surface Diffraction Beamline, ESRF—The European Synchrotron, 71 Avenue des Martyrs, 38400 Grenoble, France

<sup>4</sup>Acquired and analyzed all LEEM based data.

<sup>5</sup>Helped in interpreting the results and ensured financial support.

*Preprint submitted to Elsevier*

## 1. Introduction

To fully understand many of the challenges that arise in nanotechnology, one often needs to combine several ultramicroscopy techniques. Here, we combine Ultra High Vacuum Helium Ion Microscopy (UHV-HIM), Low Energy Electron Microscopy (LEEM), and intermittent contact mode Phase Imaging Atomic Force Microscopy (AFM) to resolve the surface structure of a thin silver film grown on Pt(111).

Since its introduction by Ward, Notte, and Economou [1] Helium Ion Microscopy

*June 13, 2022*

(HIM) [2, 3] has become an important microscopy technique providing high resolution images of sample surfaces. This is true for conducting as well as insulating materials. Here, we present a high resolution study that demonstrates the capability of HIM to visualize single atom high steps and surface reconstruction in an ordered metallic model system. This work is based on well known image formation mechanisms in HIM which utilize secondary electrons excited by the primary ion and ejected from the sample surface.

Low Energy Electron Microscopy [4] is a well established high resolution in-situ real time imaging method that utilizes low energy electrons to visualize the surface of dedicated samples with a lateral resolution of several nanometers.

Finally AFM is a widely used technique that has a much wider users base. Its variant known as phase contrast AFM allows to differentiate between materials with different surface or viscoelastic properties [5–7]

The Ag/Pt(111) system is a representative example of a surface confined alloy, which is widely studied in the field of surface science [8–13]. Deposition under UHV conditions of a 2ML thick Ag film on Pt(111) at room temperature followed by an annealing step above 550 K results in irreversible changes of the surface morphology [8]. These changes were identified by Brune et al. [14] using Scanning tunneling microscopy (STM) as the formation of a well-ordered periodic dislocation network, formed through material intermixing in the first two layers of the deposited film [15, 16]. The symmetry, periodicity and level of ordering of the network depends on the magnitude of material intermixing [17] which is controlled mainly by the substrate temperature during deposition. The structural

model of the network formed at 800 K was revised recently by Ait-Mansour et al. [16]. According to their model, the deposition of a 2-ML thick Ag film on Pt(111) followed by annealing at 800 K leads to the exchange of atoms between Pt(111) and the deposited Ag layer. The Pt interface layer contains Ag inclusions, whereas the expelled Pt atoms from the substrate form inclusions in the top layer of the alloy. The mixing of the atoms is limited only to fcc-stacking sites. Stacking faults are present at the Pt interface layer and the formed network has a 3-fold symmetry. Further deposition of Ag leads to the growth of a third layer which was reported to be purely silver and hexagonal in structure [16]. The formed dislocation network at the alloy-Pt(111) interface causes periodical undulations of the third and subsequent Ag layers [17].

## 2. Experimental

Helium Ion Microscopy has been performed in an ultra high vacuum (UHV) HIM [18, 19] Orion<sup>+</sup> from Carl Zeiss Microscopy. The system has a base pressure of  $2 \times 10^{-9}$  mbar. This pressure is reached thanks to a stainless steel sample chamber with CF type flanges, a modified pumping and load lock strategy, a 5000l/s titanium sublimation pump and a differentially pumped door gasket. The system is equipped with a standard Everhardt Thornley Detector to record secondary electron (SE) based images. In addition, detectors to count back scattered helium (BSHe) [20, 21] measure their energy [22, 23] and collect photons to enable ionoluminescence [24, 25] studies of materials are present. The presented images were recorded using a sample tilt of 35° to exploit channeling into the underlying bulk crystal. This is necessary to

maximise the surface contrast [26].

The samples were prepared and initially characterized in a Low Energy Electron Microscope (LEEM) Elmitec III. The used Pt(111) crystal had a miscut angle of less than  $0.1^\circ$ . Surface cleaning was done by prolonged repetitive cycles of argon ion bombardment, annealing in  $2 \times 10^{-7}$  mbar of oxygen at 800 K, and subsequent flashing to 1300 K.

High purity silver (99.995%) was deposited from a molybdenum crucible mounted in an electron beam evaporator (Omicron EFM-3). The growth of the silver layers was tracked in-situ and real time using bright-field mode [27, 28] in LEEM.

Care has been taken to minimize contamination of the sample surface while transporting it from the LEEM to the HIM vacuum chamber. However, oxidation of the film surface is most likely and could not be prevented. In a post HIM analysis in the LEEM and comparison of the results no significant changes relevant for the present study could be found.

The AFM measurements were done under ambient conditions with an Agilent 5100 AFM employing amplitude-modulation to record the topography. A MikroMasch Al back-coated NSC35  $\text{Si}_3\text{N}_4$  cantilever with a tip radius of 8 nm was used in these measurements. The resonance frequency of this cantilever type is 205 kHz and the nominal spring constant is 8.9 N/m. For the measurements an amplitude set-point of 90% was used and the oscillation amplitude was in the range between 30 nm and 40 nm.

### 3. Results

#### 3.1. Surface mounds and HIM sample alignment

Figure 1 shows low magnification images

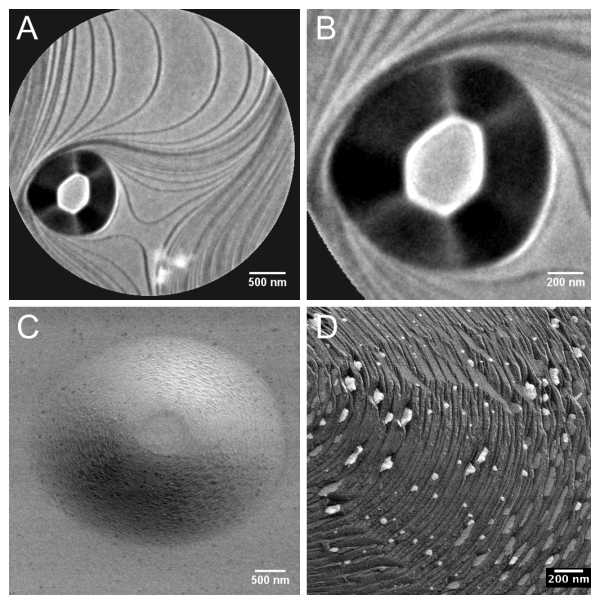


Figure 1: (A) Representative LEEM image of a hillock on the clean Pt(111) surface. The curved lines are monoatomic steps on the sample surface (electron energy 2 eV). (B) Magnification of the hillock. The hexagonal shape of the hillock is clearly visible. (C) HIM image of a Pt hillock on single crystalline Pt(111) sample covered by 3 ML equivalent of Ag. (D) High resolution scan of the mound face. The bright islands are probably Pt rich silver agglomerates, formed at the step bunches.

of the sample surface recorded by LEEM and HIM. The clean Pt(111) is occasionally decorated by hillocks which sometimes originate from screw dislocations. Representative examples of such surface mounds are presented in fig. 1. These mounds occur after annealing and a relatively swift cooling due to surface–bulk mass exchange [29]. The dark lines in fig. 1(A) are steps separating atomically flat terraces. These terraces widen significantly in the vicinity of the mound, seen as a hundreds nanometers wide dark object. These mounds are topped by a small number of atomically flat terraces which give rise to the image intensity in the mound center. This is more clearly seen in fig. 1(B) which reveals a dark line running around the top terrace, identified as an atomic step. The steps at the facets of the mound give rise to the dark contrast, caused by the small separation of the atomic steps. Additionally, it can be clearly seen in figs. 1(A) and (B) that the mound faces have different intensities forming a three–fold symmetric pattern. This difference in contrast between the individual mound facets is attributed to their particular crystallographic orientation and thus step density.

The appearance of such hillocks in HIM can be seen from figs. 1(C) and (D). A low magnification image of a mound is presented in fig. 1(C). The same threefold symmetry observed in LEEM is weakly visible. A higher magnification of the mound sidewall is shown in fig. 1(D). Using HIM images as the one presented in fig. 1(D) the orientation of the sample with respect to the beam can be determined. While in the center of the image curved step bunches are visible, straight step bunches are visible at the top and bottom of the image. These straight step bunches are preferential ori-

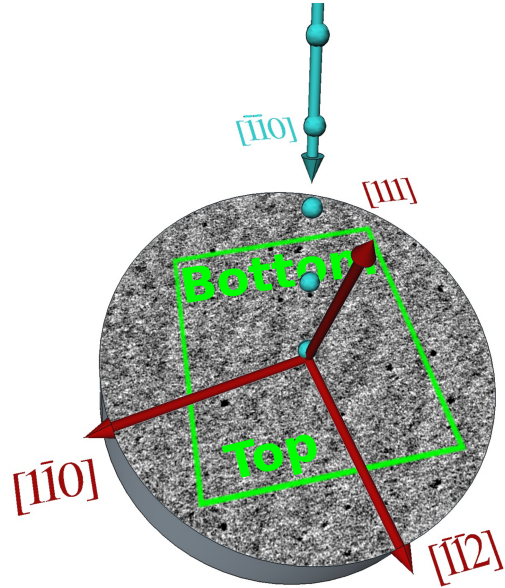


Figure 2: Sketch outlining the geometrical relation between primary He beam (light blue), sample and sample surface directions (red) relevant for the presented work. Please note that the orientation of the recorded images is upside down as indicated by the green labels.

ented parallel to the  $\langle 1\bar{1}0 \rangle$  directions of the Pt(111) sample surface. Using these step bunches the sample has been aligned with the  $\text{He}^+$  beam parallel to the  $[1\bar{1}0]$  direction and parallel to the Pt( $1\bar{1}0$ ) plane. In this channelling condition the interaction of the primary beam with the sample is minimized and results in low SE yield [18]. As a result the  $[1\bar{1}0]$  direction—except for a small alignment error—is pointing from left to right in the subsequent HIM images. The geometrical relationship between the primary He beam, the tilted sample and the crystallographic directions on the surface is outlined in fig. 2.

### 3.2. HIM step contrast

In the low magnification HIM image presented in fig. 3(A) two hillocks that originate from a twinned screw dislocation can

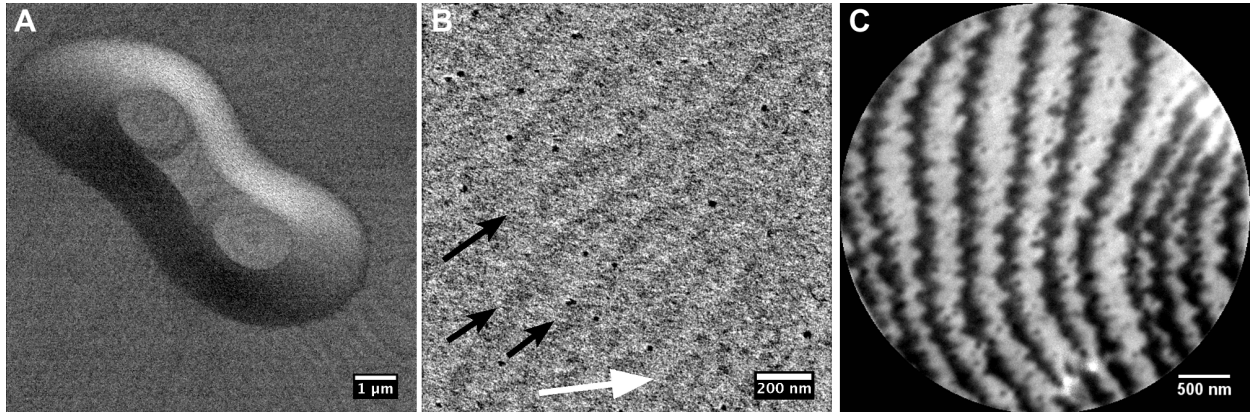


Figure 3: (A) Low magnification HIM image of a growth hillock showing step contrast. The dark curved line on top of the hillock present atomic steps. (B) High resolution detail of the Ag/Pt(111) surface showing alternating dark and bright bands. Each pair corresponds to a single terrace. Step edges are positioned at the smoother transition (indicated by a black arrow). The  $[1\bar{1}0]$  direction is indicated by the white arrow. (C) LEEM bright-field mode image recorded of the same sample showing the same alternating dark and bright bands across the terraces, energy of electrons 2 eV.

be seen. The dislocation loop cuts the surface at the centers of the mounds. On the top of the hillock dark bands can be seen. These dark bands have the typical appearance of growth steps usually found at the top of such hillocks, also observed with LEEM (fig. 1(B)) [29]. The same contrast variation can also be observed at the surface surrounding the growth mounds (see for example the lower right corner of fig. 3(A)) where micrometer sized terraces are often observed (fig. 1(A)). In fig. 3(B) a high resolution HIM image is presented obtained from the flat surface of the Ag/Pt(111) area surrounding the growth mound. A similar alternating arrangement of dark and bright bands can be observed. While from left to right the transition from bright to dark is characterized by an abrupt change in signal intensity (indicated by black arrows) the transition from dark to bright is more smooth and less straight—in some places a jagged transition line can be observed. The  $[1\bar{1}0]$  direction is indicated by a white arrow. Please note, that as expected for the

Pt(111) surface, the step edges run roughly along a  $\langle 110 \rangle$  direction, namely the  $[0\bar{1}1]$  in this case. In fig. 3(B) this direction runs roughly from bottom left to top right. The LEEM image presented in fig. 3(C) shows the same alternating bands of dark and bright signal intensity. Again two different transition lines can be distinguished. While one is characterized by triangular features the other has a straighter appearance. As the LEEM image in fig. 3(C) was recorded in bright-field mode, the difference in the contrast is caused by the significantly distinct composition of the second and third layer of the mixed silver film resulting in the different electron reflectivity from the regions covered by those layers [30].

The bright phase visible in fig. 3(C) is attributed to the second layer of the alloy which consists, according to Secondary Ion Mass Spectroscopy [16] measurements, of 22% Pt atoms in a silver matrix. The constituent of the third layer is mainly Ag. Characteristically the third layer propagates by step edges, forming a period-

ically undulated sawtooth-shaped growth front [30].

The measurement of the relative surface work-function (WF) with LEEM can be achieved with high lateral resolution by measuring the local brightness variation from a set of images recorded at different start voltages. At a very low start voltage, the probing electrons undergo total reflection (mirror mode imaging) [27, 28] resulting in uniformly bright images. With increase of the start voltage a sharp decrease in the reflected intensity is observed as electrons have enough energy to overcome the potential barrier and interact with the sample. The value of this critical voltage is a local measure of the surface WF. To measure the difference of the surface WF between two points, sets of LEEM images as a function of the start voltage were recorded. From the obtained sets, the I-V curve of each pixel was extracted.

Following the approach discussed above a work function difference between the dark and the bright bands of 25 meV has been obtained (see fig. 4). The dark spots visible in figs. 3(B,C) are attributed to platinum precipitates found in the Ag/Pt surface alloy layer.

Increasing the magnification further reveals more features of the sample surface. Three sets of parallel lines running almost horizontally and under  $\pm 120^\circ$  can be seen in the HIM image presented in fig. 5(A) (A set of lines under the observed orientation is placed in the lower left corner to help the reader). An FFT of the image is provided in fig. 5(B). Ignoring the vertical distortion—which will be discussed later—a 6 fold symmetric pattern can be observed. The spacing of the spots in the FFT is at  $6.65 \text{ nm} \pm 0.08 \text{ nm}$ . From the orientation of the spot pattern it is clear that this dis-

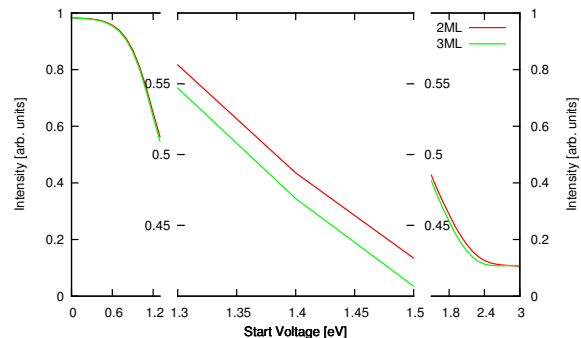


Figure 4: IV curves recorded from 2 ML (red) of Ag/Pt(111) alloy and 3 ML (green). The central part of the curve is expanded, both in x and in y-directions. The work function difference (WF) is approximately 25 meV.

tance is along the  $\langle \bar{1}\bar{1}2 \rangle$  set of directions. Please note that both the white arrow in fig. 5(A)—indicating the  $[1\bar{1}0]$  direction—as well as the FFT pattern in fig. 5(B) are slightly rotated off the horizontal due to a small azimuthal misalignment of the sample (please see fig. 2 for a sketch of the used imaging geometry). However, due to the relatively low beam energy of 30 keV the acceptance angle for channeling is sufficiently large to allow for an effective channeling through the first few nanometers [18].

### 3.3. AFM data

AFM data of a mound, recorded ex-situ after the deposition of 3 ML of Ag, are presented in fig. 6. The 3D representation of the topography data, shown in fig. 6, is shaded using the phase signal. It confirms the HIM and LEEM observations. The mound and its surrounding are decorated by small black spots. They are attributed to the platinum-rich precipitates also visible in HIM and LEEM images (see fig. 3(B)-(C) for comparison) as dark objects. Formation of those precipitates was observed in previous investigations [30, 31] upon comple-

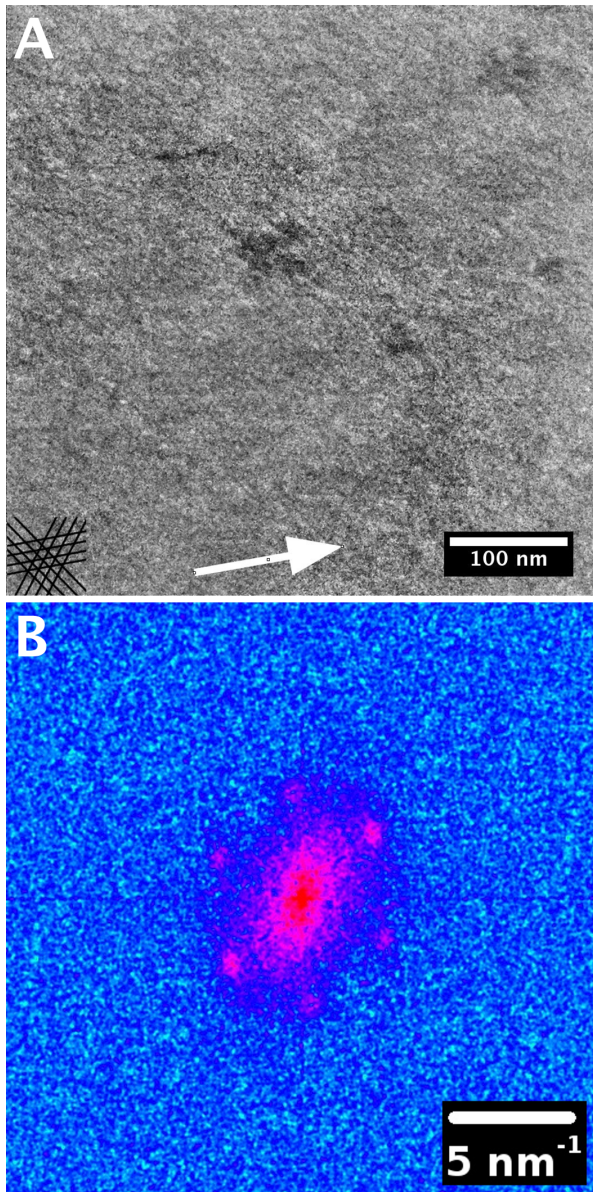


Figure 5: (A) High resolution HIM image of the Ag/Pt(111) surface. Three sets of densely packed parallel lines rotated by  $120^\circ$  can be seen. The dark irregular spots are platinum rich precipitates in the otherwise silver rich surface layer. (B) FFT of fig. 5(A). The vertical distortion in the FFT is a result of the  $35^\circ$  polar angle between sample surface and image plane. The scale bar corresponds to 5 nm real space distance measured from the center of the figure.

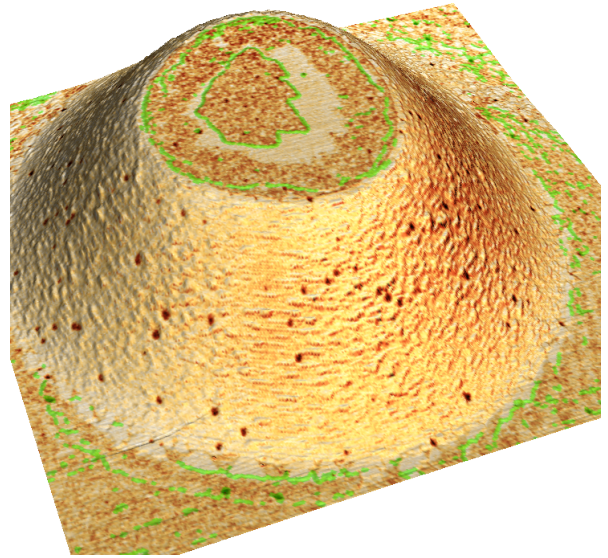


Figure 6: 3D projection of a 120 nm high surface mound recorder with AFM. The topography data has been shaded using the phase signal to reveal changes in surface termination. Step edges extracted from the amplitude signal are indicated by green lines. (FOV:  $5\mu\text{m}$ )

tion of the first layer, and were identified there, as few atoms high Pt clusters embedded in the surrounding. The clusters become less abundant but persist on the surface until a few tens of monolayers of Ag are deposited. The key observation from the data presented in fig. 6 is that the top of the mound shows regions corresponding to two different phases. One is the area appearing dark in the AFM phase data which occupies the center and rim area of the mound, the other phase is represented in white and found in between the dark areas. The fact that we can observe Pt clusters embedded in both types of regions, means that both regions correspond to at least one layer of the alloy. The sharp jagged border separating the inner—in phase contrast dark—area from the—in phase—brighter middle area represents a step edge. This separates a Pt-rich (bright) from a Ag-rich (dark)

area. This mainly triangular step edge of the center terrace is characteristic for the growth of the third and higher layers, as observed by LEEM (see fig. 3(C)) [30, 31]. The higher coverage on top of the mound is explained by steering induced flux enhancement at protrusions [32]. The diffuse border separating the bright (Pt-rich) area from the outer dark (Ag-rich) area represents the growth front of the surface alloy.

#### 4. Discussion and conclusions

Helium Ion Microscopy is well known for its surface sensitivity [26]. The usually obtained SE images are sensitive to small variations in work function [20, 33, 34]. Both effects are related to the particularities of the SE generation in HIM [35, 36]. The work function difference (see fig. 4) between the platinum rich (dark) and silver rich (bright) areas (see fig. 3(A)-(B)) is only 25 meV. This is a remarkable example for both the surface sensitivity as well as the susceptibility of the method to changes in the work function. Although the steps can not be seen directly from the morphology this is the first visualization of a single atomic layer high steps in a SE HIM image. Previous—topography based—images of steps [34] are obtained from materials with large unit cells where each step is several atoms high.

The results presented in fig. 5 are a demonstration of the applicability of the dechanneling contrast [20]. The 2 ML Ag on Pt(111) system is characterized by a stress induced triangular network of dislocations. These dislocations separate areas in the first two monolayers which are shifted along the  $[11\bar{2}]$  direction over  $1/\sqrt{3}$  of the nearest neighbour distance. Locally, this leads to a different stacking of the layers as compared

to the bulk fcc stacking. A detailed characterization of this system with respect to the surface can be found in [16, 17]. Using the step bunches on the growth hillocks (see fig. 1(A)) the sample has been aligned azimuthally with the  $[1\bar{1}0]$  direction roughly parallel to the tilt axis direction. Using a tilt of  $35^\circ$  the substrate has been oriented in a  $\langle\bar{1}\bar{1}0\rangle$  channeling direction for the incoming  $\text{He}^+$  beam. In hcp areas the top two atomic layers of the surface are shifted by two thirds of the  $\langle\bar{1}10\rangle$  inter chain spacing leading to local CAC (hcp) stacking in stead of local ABC (fcc) stacking. This closes the channel and results in an increased scattering probability. Subsequently, a higher SE yield is obtained in such hcp areas compared to the fcc areas with a lower scattering probability. The value of  $6.65\text{ nm}\pm 0.08\text{ nm}$  for the periodicity of the surface pattern is in excellent agreement with the  $6.55\text{ nm}$  measured by SPA-LEED [17]. Both values correspond to the distance between parallel base vectors of the super cell. The numbers show that the calibration of the HIM is correct to about 1%. To our surprise this also demonstrates that in this situation HIM was able to pick up the positions of atoms with atomic precision.

In summary we have—to the best of our knowledge—for the first time visualized single atom high surface steps using Helium Ion Microscopy. The contrast is based on minute changes of the work function across the otherwise atomically flat terraces. In addition we used the dechanneling contrast mechanism to successfully visualize the periodic arrangement of fcc and hcp regions in a 2 ML thick surface film. This pattern is the result of a triangular dislocation network at the interface between the silver alloy layer and the platinum bulk. The contrast in HIM is the result of a lateral dis-



placement of the outermost film layers over a nearest neighbour distance divided by  $\sqrt{3}$  along a  $\langle 11\bar{2} \rangle$  direction. The measured periodicity of 6.65 nm and the fact that the contrast is based on channeling/dechanneling confirms in detail earlier measurements using other methods. The obtained results are powerful demonstrations of the surface sensitivity and high resolution capabilities of the Helium Ion Microscopy.

## Acknowledgements

We want to thank Robin Berkelaar for acquiring the AFM data. This work is part of ECHO research program 700.58.026, which is financed by the Chemical Sciences Division of the Netherlands Organisation for Scientific Research (NWO).

## References

- [1] B. W. Ward, J. A. Notte, N. P. Economou, Helium ion microscope: A new tool for nanoscale microscopy and metrology, *J. Vac. Sci. Technol. B* 24 (6) (2006) 2871. doi:10.1116/1.2357967.
- [2] G. Hlawacek, V. Veligura, R. van Gastel, B. Poelsema, Helium ion microscopy, *J. Vac. Sci. Technol. B Microelectron. Nanom. Struct.* 32 (2) (2014) 020801. arXiv:1311.1711v1, doi:10.1116/1.4863676.
- [3] D. C. Joy, Helium Ion Microscopy, Springer-Briefs in Materials, Springer New York, New York, NY, 2013. doi:10.1007/978-1-4614-8660-2.
- [4] E. Bauer, LEEM Basics, *Surf. Rev. Lett.* 5 (6) (1998) 1275–1286.
- [5] M. Whangbo, G. Bar, R. Brandsch, Qualitative relationships describing height and phase images of tapping mode atomic force microscopy. An application to micro-contact-printed patterned self-assembled monolayers, *Appl. Phys. A* 66 (0) (1998) 1267–1270. doi:10.1007/s003390051340.
- [6] I. Schmitz, M. Schreiner, G. Friedbacher, M. Grasserbauer, Phase imaging as an extension to tapping mode AFM for the identification of material properties on humidity-sensitive surfaces, *Appl. Surf. Sci.* 115 (96) (1997) 190–198. doi:10.1016/S0169-4332(97)80204-8.
- [7] R. Garcia, R. Magerle, R. Perez, Nanoscale compositional mapping with gentle forces, *Nat. Mater.* 6 (2007) 405–411.
- [8] A. F. Becker, G. Rosenfeld, B. Poelsema, G. Comsa, Two-dimensional microstructures of submonolayer Ag on Pt (111) induced by elastic strain, *Phys. Rev. Lett.* 70 (4) (1993) 477.
- [9] H. Röder, R. Schuster, H. Brune, K. Kern, Monolayer-confined mixing at the Ag-Pt (111) interface, *Phys. Rev. Lett.* 71 (13) (1993) 2086.
- [10] U. Strüber, J. Küppers, Spectroscopic confirmation of STM derived Ag/Pt mixing in annealed Ag submonolayers at Pt (111) surfaces, *Surf. Sci. Lett.* 294 (1) (1993) L924—L928.
- [11] P. Zeppenfeld, M. A. Krzyzowski, C. Romainczyk, R. David, G. Comsa, H. Röder, K. Bromann, H. Brune, K. Kern, Stability of disk and stripe patterns of nanostructures at surfaces, *Surf. Sci.* 342 (1) (1995) L1131—L1136.
- [12] J. Tersoff, Surface-confined alloy formation in immiscible systems, *Phys. Rev. Lett.* 74 (3) (1995) 434.
- [13] M. Jankowski, H. Wormeester, H. J. W. Zandvliet, B. Poelsema, Desorption of oxygen from alloyed Ag/Pt (111), *J. Chem. Phys.* 140 (23) (2014) 234705.
- [14] H. Brune, H. Röder, C. Boragno, K. Kern, Strain relief at hexagonal-close-packed interfaces, *Phys. Rev. B* 49 (4) (1994) 2997.
- [15] A. Bendounan, J. Braun, J. Minár, S. Bornemann, R. Fasel, O. Gröning, Y. Fagot-Revurat, B. Kierren, D. Malterre, F. Sirotti, H. Ebert, Monitoring the formation of interface-confined mixture by photoelectron spectroscopy, *Phys. Rev. B* 85 (24) (2012) 245403. doi:10.1103/PhysRevB.85.245403.
- [16] K. Aït-Mansour, H. Brune, D. Passerone, M. Schmid, W. Xiao, P. Ruffieux, A. Buchsbaum, P. Varga, R. Fasel, O. Gröning, Interface-confined mixing and buried partial dislocations for Ag bilayer on Pt(111), *Phys. Rev. B* 86 (8) (2012) 085404. doi:10.1103/PhysRevB.86.085404.
- [17] M. Jankowski, H. Wormeester, H. J. W. Zandvliet, B. Poelsema, Temperature-dependent

- formation and evolution of the interfacial dislocation network of Ag/Pt(111), *Phys. Rev. B* 89 (23) (2014) 235402. doi:10.1103/PhysRevB.89.235402.
- [18] V. Veligura, G. Hlawacek, R. van Gastel, H. J. W. Zandvliet, B. Poelsema, Channeling in helium ion microscopy: Mapping of crystal orientation., *Beilstein J. Nanotechnol.* 3 (2012) 501–506. doi:10.3762/bjnano.3.57.
- [19] R. van Gastel, L. Barriss, C. A. Sanford, G. Hlawacek, L. Scipioni, A. Merkle, D. Voci, C. Fenner, H. J. W. Zandvliet, B. Poelsema, Design and performance of a Near Ultra High Vacuum Helium Ion Microscope, *Microsc. Microanal.* 17 (S2) (2011) 928–929. doi:10.1017/S1431927611005514.
- [20] G. Hlawacek, V. Veligura, S. Lorbek, T. F. Mocking, A. George, R. van Gastel, H. J. W. Zandvliet, B. Poelsema, Imaging ultra thin layers with helium ion microscopy: Utilizing the channeling contrast mechanism., *Beilstein J. Nanotechnol.* 3 (2012) 507–512. doi:10.3762/bjnano.3.58.
- [21] R. van Gastel, G. Hlawacek, H. J. W. Zandvliet, B. Poelsema, Subsurface analysis of semiconductor structures with helium ion microscopy, *Microelectron. Reliab.* 52 (9-10) (2012) 2104–2109. doi:10.1016/j.microrel.2012.06.130.
- [22] S. Sijbrandij, J. A. Notte, L. Scipioni, C. Huynh, C. A. Sanford, Analysis and metrology with a focused helium ion beam, *J. Vac. Sci. Technol. B* 28 (1) (2010) 73. doi:10.1116/1.3271254.
- [23] G. Behan, J. F. Feng, H. Z. Zhang, P. N. Nirmalraj, J. J. Boland, Effect of sample bias on backscattered ion spectroscopy in the helium ion microscope, *J. Vac. Sci. Technol. A* 28 (6) (2010) 1377. doi:10.1116/1.3502667.
- [24] V. Veligura, G. Hlawacek, U. Jahn, R. van Gastel, H. J. W. Zandvliet, B. Poelsema, Creation and physical aspects of luminescent patterns using helium ion microscopy, *J. Appl. Phys.* 115 (18) (2014) 183502. doi:10.1063/1.4875480.
- [25] S. A. Boden, T. M. W. Franklin, L. Scipioni, D. M. Bagnall, H. N. Rutt, Ionoluminescence in the helium ion microscope., *Microsc. Microanal.* 18 (6) (2012) 1253–1262. doi:10.1017/S1431927612013463.
- [26] G. Hlawacek, I. Ahmad, M. A. Smithers, E. S. Kooij, To see or not to see: Imaging surfactant coated nano-particles using HIM and SEM, *Ultramicroscopy* 135C (2013) 89–94. arXiv:1304.7167, doi:10.1016/j.ultramicro.2013.07.010.
- [27] R. M. Tromp, M. C. Reuter, Imaging with a low-energy electron microscope, *Ultramicroscopy* 50 (2) (1993) 171–178.
- [28] E. Bauer, Low energy electron microscopy, *Reports Prog. Phys.* 57 (9) (1994) 895.
- [29] B. Poelsema, J. B. Hannon, N. C. Bartelt, G. L. Kellogg, Bulk-surface vacancy exchange on Pt(111), *Appl. Phys. Lett.* 84 (2004) 2551–2553.
- [30] M. Jankowski, Reciprocal and Real Space Investigation of Ag/Pt(111); Growth, Structure and Interaction with Oxygen, Ph.D. thesis, University of Twente (2014).
- [31] E. van Vroonhoven, Remarkable Interface Activity: A LEEM Study of Ge(001) and Ag/Pt(111) at High Temperatures, Ph.D. thesis, University of Twente (2005).
- [32] S. van Dijken, L. Jorritsma, B. Poelsema, Steering enhanced roughness during metal deposition at grazing incidence, *Phys. Rev. Lett.* 82 (1999) 4038.
- [33] A. George, M. Knez, G. Hlawacek, D. Hagedoorn, H. H. J. Verputten, R. van Gastel, J. E. ten Elshof, Nanoscale patterning of organosilane molecular thin films from the gas phase and its applications: fabrication of multifunctional surfaces and large area molecular templates for site-selective material deposition., *Langmuir* 28 (5) (2012) 3045–3052. doi:10.1021/la204437r.
- [34] K. Buchholt, P. Eklund, J. Jensen, J. Lu, A. L. Spetz, L. Hultman, Step-flow growth of nanolaminate Ti<sub>3</sub>SiC<sub>2</sub> epitaxial layers on 4H-SiC(0001), *Scr. Mater.* 64 (12) (2011) 1141–1144. doi:10.1016/j.scriptamat.2011.03.013.
- [35] K. Ohya, T. Yamanaka, K. Inai, T. Ishitani, Comparison of secondary electron emission in helium ion microscope with gallium ion and electron microscopes, *Nucl. Instruments Methods Phys. Res. Sect. B* 267 (4) (2009) 584–589. doi:10.1016/j.nimb.2008.11.003.
- [36] Y. V. Petrov, O. F. Vyvenko, Secondary electron emission spectra and energy selective imaging in helium ion microscope, in: J. T. Thomas, D. D. Desjardins, J. J. Güell,

K. L. Bernier (Eds.), Proc. SPIE, Vol. 8036,  
SPIE, Orlando, Florida, 2011, pp. 80360O-1-  
80360O-10. doi:10.1117/12.886347.